Indian Journal of Chemistry
Vol. 56A, February 2017, pp. 211-219

Synthesis, spectroscopic properties and theoretical calculations on methylene bridged 1,8-naphthyridine ligands and copper(I) complex through a non-catalyst C(sp^3)–H methylenation

Gao-Zhang Gou[a,*], Bo Zhou[a], Xue-Bing Chen[a], Xue-Quan Wang[a], Chao-Yong Mang[b], Wei Liu[a] & Shao-Ming Chi[c,*]

[a]School of Science, Honghe University, Mengzi, Yunnan 661199, PR China
Email: hhxylxyhxx@126.com (GZG)

[b]College of Pharmaceutical Science and Chemistry, Dali University, Dali, Yunnan 671000, PR China

[c]College of Chemistry and Chemical Engineering, Yunnan Normal University, Kunming 650092, PR China
Email:chishaoming@gmail.com (SMC)

Received 13 April 2016; revised and accepted 13 February 2017

Two 1,8-naphthyridine derivatives containing methylene, N-(5-methyl-7-((3-oxo-1,3-dihydroisobenzofuran-1-yl)methyl)-1,8-naphthyridin-2-yl)acetamide (**L1**) and 2-amino-3-((7-amino-4-methyl-1,8-naphthyridin-2-yl)methyl)isoindolin-1-one (**L2**), as well as a copper(I) complex $CuI(L1)_2$ (**C1**) have been synthesized through a non-catalyst C(sp^3)–H methylenation process and characterized. The structure of **C1** has been determined by X-ray diffraction analysis. The spectroscopic properties have been investigated by experimental as well as theoretical studies for all these compounds. The two ligands exhibit similar electronic absorption spectra with λ_{max} at about 340 nm, which can be tentatively assigned to $\pi_{naph}\rightarrow\pi_{naph}^*$ transition. The electronic absorption spectra of **C1** exhibits at ~335 nm except in *n*-hexane, which may be assigned tentatively to the intraligand charge transfer transition. The assignment is further supported by density functional theory calculations and cyclic voltammetry.

Keywords: Coordination chemistry, Density functional calculations, Metal-to-ligand charge-transfer, Crystal structure, Spectroscopic properties, 1,8-Naphthyridine, Copper

Naphthyridines (pyridopyridines, diazanaphthalenes) represent a group of six isomeric heterocyclic systems containing two fused pyridine rings with different mutual arrangements of nitrogen atoms. The first derivative of the cyclic naphthyridine system was obtained in 1893 by Reissert[1], who proposed this name for the new class of heterocyclic compounds. The pharmacological and medicinal applications of 1,8-naphthyridine (NP) derivatives have shaped and continue to influence the growth of NP chemistry. 1,8-Naphthyridine compounds have been extensively investigated not only due to their special conjugate π electronic structures, good coordination capabilities[2], favourable photophysical and photochemical properties[3-7], but also their potential applications as functional materials in the fields of solar energy conversion, sensors[8-10], supermolecular assemblies[11-13], photocatalysis[14, 15], nonlinear optical materials, biological activeites[16, 17] and optical molecular devices,[18-20] etc. A number of 1,8-naphthyridine derivatives[21, 22] have been synthesized since the first 1,8-naphthyridine compound was prepared in 1920s. Numerous complexes with naphthyridine-based ligands in different coordination modes have also been reported since 1969[23, 24].

Research on luminescent 1,8-naphthyridine derivatives and their Cu(I) complexes has focused on emissive $\pi\rightarrow\pi^*$ or metal-to-ligand charge-transfer (MLCT) excited states which can be tuned by hydrogen-bonding sites leading to intra- or intermolecular interactions[25]. A previous study on luminescent copper(I) and platinum(II) complexes with a flexible naphthyridine-phosphine ligand demonstrated that this class of ligand exhibits various intriguing coordination modes and bonding properties[26]. However, the studies on 1,8-naphthyridyl derivatives with flexible spacers and their metal complexes are rare. The spacers enable the ligand to rotate freely, thereby resulting in various coordination modes and interesting spectroscopic properties. Herein, we report on the synthesis and characterization of two new 1,8-naphthyridine

compounds **L1**, **L2** and a copper(I) complex $CuI(L1)_2$ (**C1**) through a non-catalyst $C(sp^3)$–H methylenation process in which the 1,8-naphthyridinyl segment and the isobenzofuran lactone group are connected by a methylene bridge (Scheme 1). Their structures and spectroscopic properties are comprehensive studied involving experimental data and time-dependent density functional theory (TD-DFT) calculations.

Materials and Methods

Synthesis and charaterisation

^{1}H NMR spectra were recorded on a Bruker Avance 500 spectrometer with tetramethylsilane (^{1}H) as an internal standard. The mass spectra were recorded on a Finnigan LCQ quadrupole ion trap mass spectrometer, with samples were dissolved in HPLC grade methanol. Elemental analyses were performed on Carlo Erba-1106 instrument. UV-vis absorption spectra were recorded using a Hitachi U-3010 spectrophotometer. Emission and excitation spectra were obtained on a Hitachi F-7000 fluorescence spectrophotometer. The fluorescence quantum yields in solution were measured relative to quinine sulfate in 0.1 *N* sulfuric acid aqueous solution (λ_{ex} = 345 nm, Φ_F = 0.546) at room temperature and calculated by $\Phi_s = \Phi_r \times \left(\frac{B_r}{B_s}\right) \times \left(\frac{n_s}{n_r}\right) \times \left(\frac{D_s}{D_r}\right)$, where the subscripts *s* and *r* refer to the sample and reference standard solution respectively, *n* is the refractive index of the solvent, *D* the integrated intensity, and *Φ* the luminescence quantum yield. The quantity *B* was calculated by $B = 1–10^{-AL}$, where *A* is the absorbance at the excitation wavelength and *L* the optical path length. Errors for wavelength values (1 nm) and Φ (10%) were estimated.

L was synthesized as follows: To a 50 mL flask, were added 7-acetamino-2,4-dimethy-1,8-naphthyridine (100 mg, 0.46 mmol), 2-carboxybenzaldehyde (84 mg, 0.56 mmol), and 40 mL of freshly distilled *N,N*-dimethylformamide. The mixture was heated with stirring for 24 h at 150 °C under nitrogen atomsphere. After cooling to room temperature, the mixture was removed under reduced pressure to obtain a pale yellow solid. The crude product was purified by chromatography on silica gel (ethyl acetate:petroleum ether = 1:1) to give L1 as pale yellow solid (105 mg, Yield: 65%). ^{1}H NMR (500 MHz, $CDCl_3$) δ 8.58 (s, 1H NH), 8.54 (d, J = 9.1 Hz, 1H Naph-H), 8.41 (d, J = 9.0 Hz, 1H Naph-H), 7.94 (d, J = 7.6 Hz, 1H Ar-H), 7.67 (t, J = 7.5 Hz, 1H Ar-H), 7.56 (t, J = 7.5 Hz, 1H Ar-H), 7.44 (d, J = 7.7 Hz, 1H Ar-H), 7.26 (s, 1H Naph-H), 6.25 (dd, J = 8.7, 4.7 Hz, 1H CH), 3.57 (dd, J = 14.5, 4.6 Hz, 1H CH_2), 3.36 (dd, J = 14.5, 8.8 Hz, 1H CH_2), 2.73 (s, 3H CH_3), 2.30 (s, 3H CH_3). ESI-MS: m/z 348.1 $[M+H]^+$. Anal. (%): calcd (%) for $C_{20}H_{17}N_3O_3$: C, 69.15; H, 4.93; N, 12.10; O, 13.82; found: C, 69.11; H, 4.89; N, 12.15.

L2 was synthesized as follows: Diamid hydrate (58 mg, 1.4 mmol) was added to a stirred solution of compound **L1** (100 mg, 0.28 mmol) in THF (15 mL). The resulting suspension was stirred and refluxed at 65 °C for 4 h. After cooling to room temperature, the reaction mixture was removed under reduced pressure to obtain a yellow solid. The crude product was purified by chromatography on silica gel (CH_2Cl_2:CH_3OH=15:1) to give **L2** as yellow solid (83 mg, Yield: 90%). ^{1}H NMR (500 MHz, $CDCl_3$) δ 8.07 (d, J = 8.9 Hz, 1H Naph-H), 7.91 (d, J = 7.6 Hz, 1H Naph-H), 7.63 (t, J = 8.0 Hz, 1H Ar-H), 7.52 (t, J = 7.5 Hz, 1H Ar-H), 7.42 (d, J = 7.6 Hz, 1H Ar-H), 7.03 (s, 1H Naph-H), 6.81 (d, J = 8.9 Hz, 1H Ar-H), 6.23 (dd, J = 8.7, 4.8 Hz, 1H CH), 5.26 (s, 2H NH_2), 3.43 (m, 1H CH_2), 3.28 (dd, J = 14.2, 8.7 Hz, 1H CH_2), 2.60 (s, 3H CH_3), 1.82 (s, 2H NH_2). ESI-MS: *m/z* 320.3 $[M+H]^+$. Anal. (%): calcd for $C_{18}H_{17}N_5O$: C, 67.70; H, 5.37; N, 21.93; O, 5.01; found: C, 67.65; H, 5.41; N, 21.89.

For synthesis of the copper(II) complex, **C1**, the ligand **L1** (0.072 g, 0.2 mmol) and CuI (158 mg, 0.8 mmol) were mixed with stirring in dichloromethane (25 mL) under a nitrogen atmosphere at room temperature for 24 h. The resulting solution was filtered and the solvent was removed *in vacuo* to yield a yellow precipitate. The deep brown prism crystals suitable for X-ray diffraction were obtained by diffusion of diethyl ether into a dichloromethane solution. Yield: (65 mg, Yield: 36%). The yellow crystalline solid was characterized by elemental analysis and X-ray crystallography. ESI-MS: *m/z* 757.4$[M-I]^+$. Anal. (%): calcd for $C_{40}H_{34}CuIN_6O_6$: C, 54.27; H, 3.87; Cu, 7.18; I, 14.34; N, 9.49; O, 10.84; found: C, 54.21; H, 3.89; N, 9.47.

XRD analysis

Single crystals of **C1** suitable for X-ray diffraction analysis were grown by slow diffusion of diethyl ether vapors into a dichloromethane solution. The diffraction data were collected on a Rigaku R-AXIS RAPID IP X-ray diffractometer using a graphite monochromator

with Mo-Kα radiation (λ = 0.071073 nm) at 293 K. The structures were solved by direct methods and refined by full-matrix least-squares methods on all *F2* data (SHELX-97) [27]. Non-hydrogen atoms were refined anisotropically. The positions of hydrogen atoms were calculated and refined isotropically. A summary of the crystallographic parameters and data is given in Tables S1, S2, S3 and S4.

Cyclic voltammetric studies

Cyclic voltammetry experiments were performed with a computer controlled CHI660E electrochemical workstation. Typical electrochemical cells consisted of three-electrode setup including a glassy carbon working electrode, platinum counter electrode, and SCE as quasi-reference electrode. Dichloromethane solutions of the analyte (1.0 mmol L^{-1}) and electrolyte (0.10 mol L^{-1} $^nBu_4NPF_6$) were scaned rate at 100 mV s^{-1} (refs 28-30). The potentials for the waves were observed in the +2.0 V to –1.8 V window.

Density functional theory calculations

Gaussian 09W package[31] was used in the present computational study. All geometrical structures were fully optimized without the symmetric restraint using the DFT method[32,33] combined with the Becke, three-parameter, Lee-Yang-Parr (B3LYP) exchange-correlation functional[34-36] with the 6-311++G** basis set[37-40] for H, C, N, O atoms and LANL2DZ[41] effective core potentials and basis set for Cu and I atoms. The electronically excited states involving the first 30 excited states were calculated by using the TD-DFT method. In all the calculations, squeezed self-consistent field (SCF) convergence standards, the self-consistent reaction field (SCRF) method and polarized continuum model (PCM)[42] were adopted. The UV-vis spectra were computed from TD-DFT calculations in different solvents (gas, CH_2Cl_2, DMF) and molecular orbitals calculated in gas phase.

Results and Discussion

Synthesis and characterisation

The naphthyridine precursor **1** was prepared from 2,6-diaminopyridine in a two-step synthetic route by literature methods[43-47]. **L1** was the product of the reaction between **1** and 2-carboxybenzaldehyde in dry *N,N*-dimethylformamide at 150 ºC (the expected ethylene **3** was not formed, possible because there was no catalyst or dehydrant) (Scheme 1). This is the first report of synthesis of new 1,8-naphthyridine-lactone ligands through a non-catalytic C(sp^3)–H methylenation process[48] although there are some reports in the literature on activation of C(sp^3)–H bond to aldehyde using special catalysts like acidic ionic liquids, indium trichloride and cobalt[49-53]. The structures of **L1** and **L2** were characterized by multinuclear NMR spectroscopy, mass spectroscopy and elemental analyses (Figs S1, S2). A broad peak is observed at about 9.01 ppm in the ^{1}H-NMR spectroscopy of **L1**, which is an indication of the NH proton of the acetamido group. However, in the ^{1}H-NMR spectroscopy of **L2,** there are two broad peaks

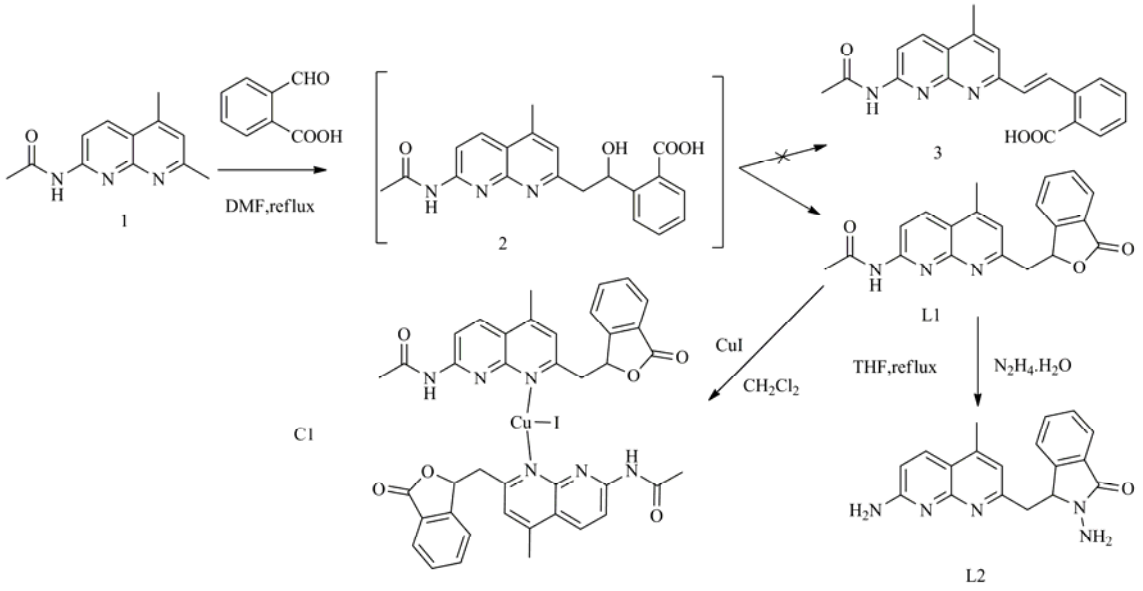

Scheme 1

at about 5.26 and 1.82 ppm, which indicate the NH_2 proton. The amino proton (R-NH_2) can appear over a wide range of 0–4 ppm. In the present study, the peak at 5.26 ppm is the amino proton on the naphthyridine ring and that at 1.82 ppm is the amino proton on the lactam unit. In similar structures, the amino proton has been reported to appear at ~3.0 ppm[54].

Furthermore, mass spectrum and elemental analyses revealed that compounds **L1** and **L2** are bridged by methylene. This is also confirmed by the crystal structure of **C1**. Crystal structure of **C1** is depicted in Fig. 1 and detailed crystallographic data is gathered in Table S1. Bond lengths, angles, torsion angles and hydrogen bonds are given in Tables S2-S4. Complex **C1** crystallizes in the triclinic space group *P*2(1)/*c*. The structure reveals a coplanar triangle geometry around the Cu(I) ions which is bound to two N-atom from the naphthyridine ring of **L1** and one I-atom. The dihedron angle between the benzofuran lactone ring and the naphthyridine plane is about 35.9º, 1.8º for two benzofuran lactone rings and 32.7º for two naphthyridine plane (Fig. S3). The distances of N(1)-Cu(1), N(4)-Cu(1) and I(1)-Cu(1) are respectively 2.054, 2.048 and 2.511 Å. The bond angles at the copper atom are 113.2º, 120.5º and 126.2º. Complex **C1** contains two intramolecular hydrogen bonds of length 2.37 Å for H(3A)…O(4) and 2.32 Å for H(6A)…O(1), while the N(3)-O(4) and N(6)-O(1) distances are 3.22 and 3.17 Å, respectively (Fig. S3, Tables S2, S3, S4). Surprisingly, the Cu-atom of **C1** is coordinated to the coplanar triangle geometry with all the atoms being connected to each other through single bonds. The Cu-atom is located in the center of the triangle. The unusual coordination mode for the complex has not been reported in the literature to the best of our knowledge.

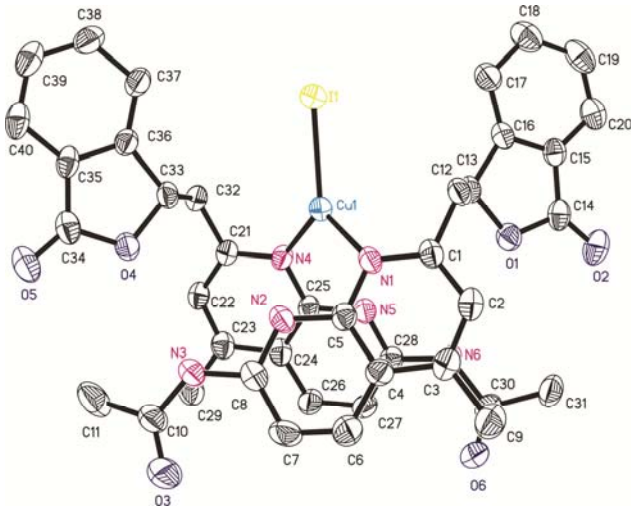

Fig. 1 – ORTEP diagrams for C1 showing 30% probability ellpsoids. All H-atoms are omitted for clarity.

Reaction mechanism

The above synthesis reaction process may be proceeding via the transition state intermediate compound **2** (see in Scheme 1). Density functional theory (DFT) calculations were carried out to investigate the compound **L1**, substrate **1**, transition state intermediate compound **2** and the expected compound **3** in the reaction. The relative energies calculated at 6-311++G** level in different solvents of **L1**, **1**, **2**, **3** are shown in Fig. 2. Based on the relative energy of **1** as indicator, the relative energies of compounds **L1** and **3** are similar and smaller than that of **2**. Hence, **L1** and **3** can be generated theoretically from the transition state intermediate compound **2**, but since there was no special catalyst or dehydrating agent in the reaction, only compound **L1** was produced. The reaction mechanism is shown in Scheme 2. The α-H is removed from the Me-naphthyridine group by compound **1** to form a carbanion. Then the carbanion attacks the carbon atom of aldehyde group to generate the transition state intermediate **2**, followed by the intramolecular esterification reaction. In order to verify the reaction process and mechanism, the molecular atomic charges of naphthyridine precursor **1** were calculated using the same method. As shown in Fig. 3, the charges of Me unit in compound **1** are −0.408, −0.460 and −0.471,

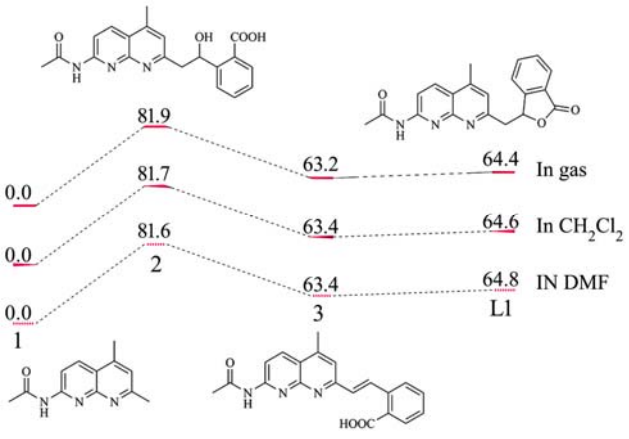

Fig. 2 – DFT optimized structures and relative energies (Hartree) of **1**, **2**, **3** and **L1** at 6-311++G** level in different solvents.

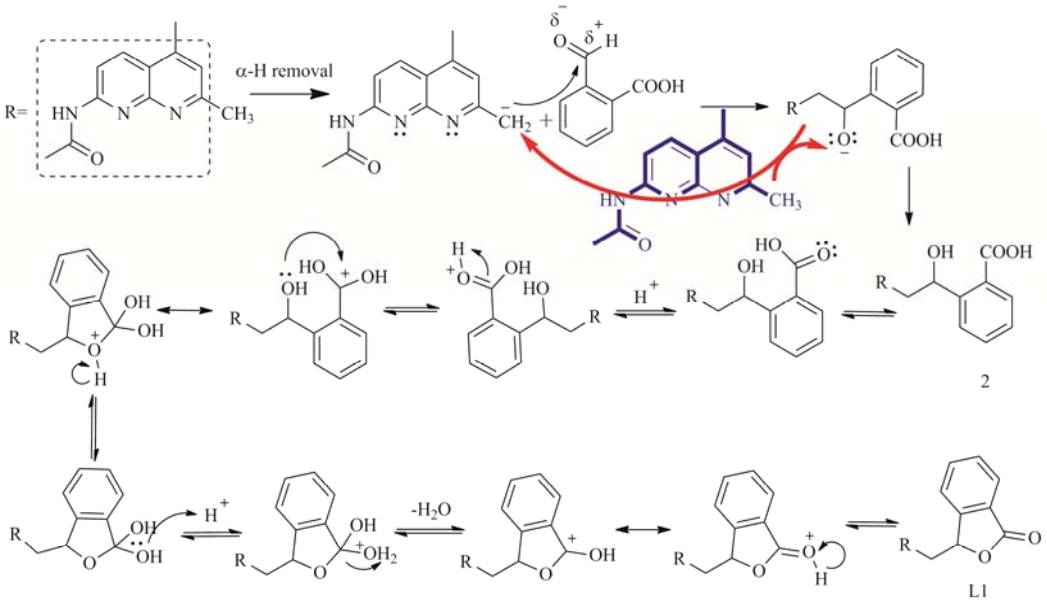

Scheme 2

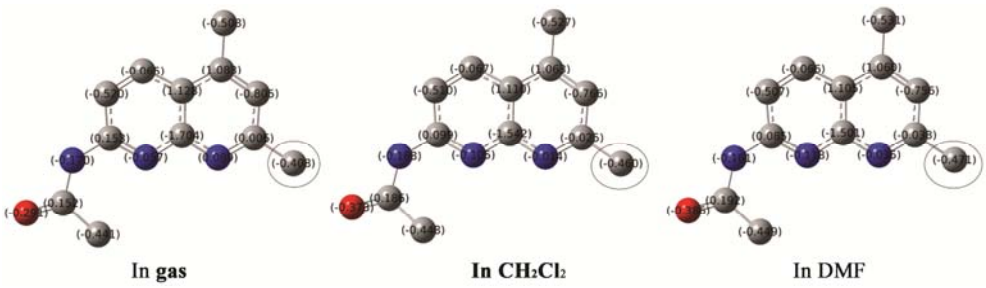

Fig. 3 – DFT optimized structures and atomic charge of **1** at 6-311++G** level in different solvents.

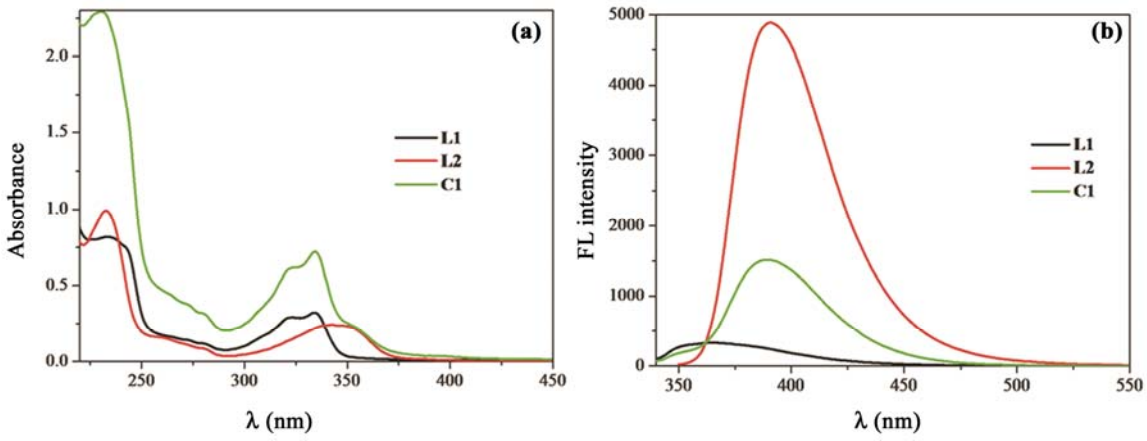

Fig. 4 – (a) UV-vis absorption and (b) emission spectra of **L1**, **L2** and **C1** in MeOH measured at a concentration of ~1.0×10^{-5} mol L^{-1}.

Table 1 – Optical properties of **L1**, **L2** and **C1** in various solvents at 298 K

Comp.	Solvent	λ_{ab} (nm) (ε, mol^{-1} dm^3 cm^{-1})	λ_{em} (nm)	Stokes shift (nm)	λ_{em} (nm)[a]	Φ_f[b]
L1	*n*-Hexane	336	411	75	418	0.05
	CH_2Cl_2	322, 335	361, 399, 419	84		0.03
	CH_3CN	321, 334	364, 400, 407	73		0.05
	MeOH	334 (15592)	365	31		0.03
L2	*n*-Hexane	346	386, 399	53	482	0.10
	CH_2Cl_2	336	378	42		0.41
	CH_3CN	339	382	43		0.40
	MeOH	343 (12130)	390	47		0.42
C1	*n*-Hexane	373	393, 415	42	n.d.	0.09
	CH_2Cl_2	322, 335	360	25		0.07
	CH_3CN	321, 334	362	28		0.07
	MeOH	334 (41570)	389	55		0.11

[a]Solid; [b]φ = fluorescence quantum yield, calculated using quinine sulfate as standard (φ = 0.546 in 0.5 mol/L H_2SO_4).

respectively. This indicates that the Me unit of compound **1** forms carbanions easily and attacks the aldehyde group in the reaction solvent, i. e. *N,N*-dimethylformamide.

Electronic absorption spectroscopy and photoluminescence

The spectral properties of compounds **L1**, **L2** and **C1** were examined under various conditions and the results are summarized in Table 1. As shown in Fig. 4, compounds **L1**, **L2** and **C1** in methanol exhibit moderately intense absorptions at 300-375 nm and intense bands between 225 and 250 nm. The structured low-energy absorption bands with a large extinction coefficient (~10^4 mol^{-1} dm^{-3} cm^{-1}) may be assigned to the 0→0 vibrational band of the strong $S_0 \rightarrow S_1$ transition with some charge-transfer character, as evidenced by the slight sensitivity towards solvent polarity (Fig. S4). Comparing **L1** and **L2**, introduction of the NH_2 unit causes a significant shift (11 nm) in the absorption maximum, but not in the case of **C1**.

Upon excitation at 335 nm, the emission spectra of **L1**, **L2** and **C1** in methanol feature a broad and structureless peak, with λ_{max} at 365 nm (quantum yield 3%; Stokes shift 31 nm) , 390 nm (42%; 47 nm) and 389 nm (11%; 55 nm), respectively (Table 1). Although the emission bands in **L2** and **C1** occur at almost the same position, the quantum yield of the former is obviously higher relative to the latter. This may be due to their analogous-extended structures and distinct photoluminescence mechanism. The emission intensity of **L2** is strongly dependent on solvents and increases markedly with increase in solvent polarity (Fig. S4). In the polar solvent, the n→π* transition energy increases and the π→π* transition energy decreases, which leads to the fluorescence enhancement and fluorescence peak red shift. More

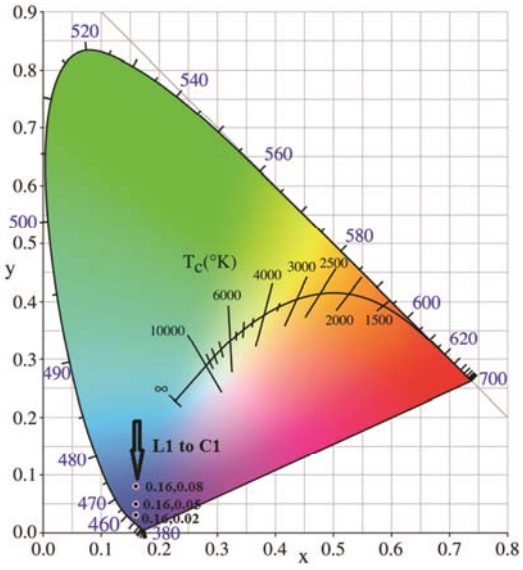

Fig. 5 – CIE-1931 chromaticity diagram of **L1**, **L2** and **C1**.

than 29-fold enhancement in fluorescence intensity was recorded when the extremes of methanol and *n*-hexane were compared (Fig. S4). Further, the fluorescence intensity of **L1** is insensitive to solvents and the maximum of the low-energy absorption band of **L1** is blue-shifted about 46 nm in methanol. On the other hand, the fluorescence intensity of **C1** is most sensitive to solvents especially in dichloromethane to methanol except in *n*-hexane; this may be rationalized by the fact that the introduction of the Cu(I) in **C1** leads to the intraligand charge transfer (ILCT) transition (π_{naph}–π_L*)[23]. The Commission Internationale de L'Eclairage (CIE) coordinates of (0.16, 0.08) for **L1**, (0.16, 0.05) for **L2** and (0.16, 0.02) for **C1** is consistent with the international standard blue coordinates (0.16, 0.01) (Fig. 5).

Upon titration of **L1**, **L2** and **C1** with HBF_4 as a proton source in CH_3OH, the absorptions of **L1**, **L2** and **C1** have no significant change, but all of them appear as isosbestic points (Fig. S5). The hydrogen ion associated with the naphthyrine moiety promotes the π_{ben}-π_{napy}* transition[23]. However, **L1** and **C1** exhibit an attenuate emission with λ_{max} at about 375 nm upon excitation at 335 nm at room temperature while the emission of **L2** is inconspicuous when titrated with HBF_4 as a proton source in CH_3OH (Fig. S5). The variation is observed on titration of HBF_4 with 5.0 equiv. of **L1** and 2.5 equiv. of **C1**. The luminescence intensity was measured as a function of HBF_4 concentration and decreased with an increase in the degree of protonated nitrogen atoms on the naphthyridine ring. This is useful for decreasing the ICT transition energies. The titration study for **L1, L2** and **C1** with HBF_4 is meaningful for investigations into the acid-controlled molecular switch from the luminescence intensity change caused by proton source using this kind of 1,8-naphthyridine compounds.

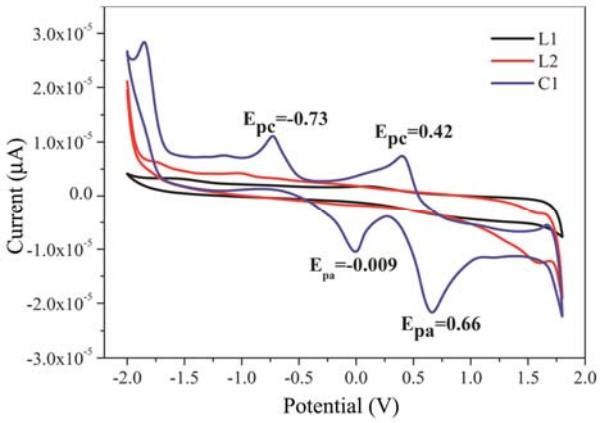

Fig. 6 – Cyclic voltammagrams for **L1**, **L2** and **C1** in dichloromethane using 0.1 mmol L^{-1} *n*-Bu_4NPF_6 as supporting electrolyte and scan rate of 100 mV s^{-1}.

Electrochemical studies

The electrochemical properties of **L1**, **L2** and **C1** were studied by cyclic voltammetry in dichloromethane solution with tetrabutylammonium hexafluorophosphate as supporting electrolyte. The resulting cyclic voltammograms are presented in Fig. 6. Compound **L1** and **L2** exhibit inconspicuous irreversible reduction wave, while **C1** exhibits an irreversible oxidation wave ($E_{½}^{OX}$ = +0.54 V, ΔE_p = 0.24 V) and a reversible oxidation wave ($E_{½}^{OX}$ = +0.36 V, ΔE_p = 0.72V), which can be assigned to a one-electron oxidation and a one-electron reduction of the ligand unit, respectively. In other words, coordination of **C1** with two ligand unit does not perturb the reduction potential, but the reducing capacity was strengthened and appeared as an irreversible oxidation peak. For **C1**, the reversible reduction is attributed to the formation of stable naphthyridine ligand radical anions.

Density functional theory calculations

To gain a deeper insight into the observed spectroscopic properties of **L1**, **L2** and **C1**, density functional theory calculations were performed on these compounds with the Gaussian 09W package[31]. All geometrical structures were optimized with the 6-311++G** basis set for H, C, N, O atoms and LANL2DZ effective core potential basis set for Cu, I atoms. UV-vis spectra were computed from TD-DFT calculations in different solvents (gas, CH_2Cl_2, DMF) and molecular orbitals calculated in gas.

As shown in Fig. S6 and Table 2, the calculated values of the maximum absorption wavelengths (307 nm for **L1** and 321 nm for **L2** and 350 nm for C1 in CH_2Cl_2) agree well with the experimental results. The deviation of maximum absorption wavelengths between experimental and computational values was

Table 2 – Absorption maxima, main orbital transitions and oscillator strengths of **L1**, **L2** and **C1** calculated in different solution

Comp.	Solution	Electronic transitions	Energy (eV)	λ_{ab} (nm)	λ_{ab} (nm)[a] (error ratio, %)	Main orbital transitions	Oscillator strengths (*f*)
L1	In gas	$S_0 \rightarrow S_2$	4.08	303.5	322	HOMO to LUMO(83.8%)	0.19
	In CH_2Cl_2	$S_0 \rightarrow S_1$	4.04	306.8	(4.9%)	HOMO to LUMO(91.2%)	0.34
	In DMF	$S_0 \rightarrow S_1$	4.03	307.7		HOMO to LUMO(91.5%)	0.37
L2	In gas	$S_0 \rightarrow S_1$	3.93	315.5	336	HOMO to LUMO(91.4%)	0.18
	In CH_2Cl_2	$S_0 \rightarrow S_1$	3.85	322.1	(4.1%)	HOMO to LUMO(94.2%)	0.29
	In DMF	$S_0 \rightarrow S_1$	3.85	321.9		HOMO to LUMO(94.2%)	0.29
C1	In gas	$S_0 \rightarrow S_{17}$	3.23	383.4	322	HOMO-3 to LUMO+1(71.3%)	0.02
	In CH_2Cl_2	$S_0 \rightarrow S_{24}$	3.93	315.7	(2.1)%	HOMO-1 to LUMO+5(59.5%)	0.11
	In DMF	$S_0 \rightarrow S_{24}$	3.96	312.6		HOMO-7 to LUMO (63.0%)	0.25

[a]Experimental values measured in dichloromethane.

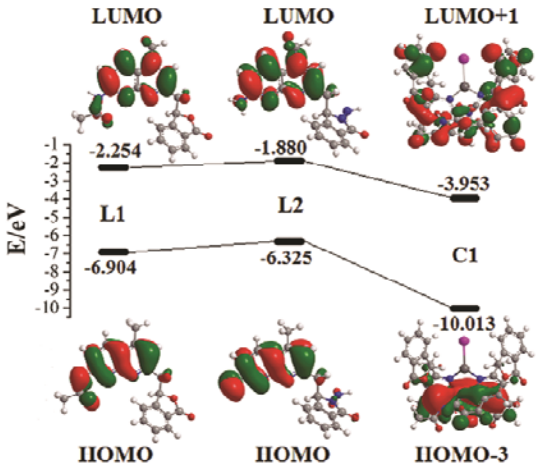

Fig. 7 – The main molecular orbital energy diagram and isodensity surface plots of **L1**, **L2** and **C1** calculated in gas.

about 15 nm (4.5%). Figure 7 shows the electron distribution of the LUMO and HOMO for **L1**, **L2**, **C1** with the related data given in Table 2. Clearly, the LUMO densities in **L1** and **L2** are mainly located on the naphthyridine moiety and the HOMO densities on the naphthyridine fragment (Fig. 7). This is further suggestive of some charge-transfer character, confirming that the ICT from the naphthyridine ring to the naphthyridine moiety does take place for **L1** and **L2**. The maximum absorption wavelengths of **L1** and **L2** are contributed by the $S_0 \rightarrow S_1$ transition arising from the HOMO to LUMO ($\pi_{naph} \rightarrow \pi_{naph}^*$) transition. The LUMO energy level of **L1** (–2.254 eV) and **L2** (–1.880 eV) are almost the same, while the HOMO level of **L2** (–6.325 eV) is slightly low relative to **L1** (–6.904 eV). In sharp contrast, the HOMO-3 density of **C1** is restrained over the naphthyridyl ring and the LUMO+1 density is delocalized over the entire molecule. However, the HOMO receives contributions mainly from naphthyridyl ring and the LUMO mainly from entire ligand group, suggestive of some charge-transfer character from the naphthyridine moiety to the ligand group. The maximum absorption wavelengths of **C1** is contributed by the $S_0 \rightarrow S_{24}$ interaction from HOMO-3 to LUMO+1 ($\pi_{naph} \rightarrow \pi_L^*$) transition. The LUMO energy level of **C1** is –3.953 eV and the HOMO energy level is –10.013 eV. The tendency for the calculated HOMO and LUMO energy levels are consistent with the observations from cyclic voltammetry.

Conclusions

We describe herein the syntheses, structures, spectroscopic and electrochemical properties of two new 1,8-naphthyridine derivatives (**L1**, **L2**) bridged by methylene and a copper(I) complex $CuI(L1)_2$ (**C1**). The possible mechanism of the reaction for **L1** was studied by density functional theory calculations. The results showed that compound **L1** could be produced even without a special catalyst or dehydrating agent in the reaction. The two ligands exhibited similar electronic absorption spectra with λ_{max} at about 340 nm that can be tentatively assigned to $\pi_{naph} \rightarrow \pi_{naph}^*$ transition from HOMO to LUMO, which is further supported by the density functional theory calculations and cyclic voltammetry data. Titrations of **L1**, **L2** and **C1** upon addition of HBF_4 in CH_3OH were studied. The understanding of the spectroscopic properties of **L1**, **L2** and **C1** will be beneficial for the design of novel 1,8-naphthyridine compounds and their applications in ions sensing such as in designing of acid-controlled molecular switches.

Supplementary Data

CCDC 1529689 contains the supplementary crystallographic data for **C1**. These data can be obtained free of charge from the Cambridge Crystallographic Centre, 12 Union Road, Cambridge CB21EZ, UK; Fax: (+44) 1223–336033; via www.ccdc.cam.ac.uk/data_request/cif or deposit@ccdc.cam.ac.uk. Other supplementary data associated with this article, i. e., characterization data, computational details, additional spectral data, and crystallographic data are available in the electronic form at http://www.niscair.res.in/jinfo/ijca/IJCA_56A(02)211-219_SupplData.pdf.

Acknowledgement

This work is supported by the National Natural Science Foundation of China, PR China (61361002 and 21262049), the “Chun Hui” Plan of Chinese Ministry Education, PR China (Z2011125), the Scientific Research Foundation of Education Department of Yunnan Province, PR China (No. 2013FZ121), the General Program of Yunnan Provincial Education Department, PR China (2015Y455), the Chemistry of Key Construction Disciplines for Master Degree Program in Yunnan, PR China (No. HXZ1303) and the Educational Reform Program of Honghe University, PR China (No. JJJG1412).

References

1 Mogilaiah K, Shiva P R & Kumara S J, *Indian J Chem*, 49B (2010) 335.
2 Bera J K, Sadhukhan N & Majumdar M, *Eur J Inorg Chem*, 2009 (2009) 4023.
3 Litvinov V, *Adv Heterocycl Chem*, 91 (2006) 189.
4 Paudler W W & Sheets R M, *Adv Heterocycl Chem*, 33 (1983)147.
5 Andrews M, Laye R H & Pope S J, *Trans Metal Chem*, 34 (2009) 493.
6 Litvinov V P, Roman S V & Dyachenko V D, *Russian Chem Rev*, 69 (2000) 201.
7 Araki H, Tsuge K, Sasaki Y, Ishizaka S & Kitamura N, *Inorg Chem*, 46 (2007) 10032.
8 Wang C X, Sato Y, Kudo M, Nishizawa S & Teramae N, *Chem-Eur J*, 18 (2012) 948.
9 Li Z X, Zhao W Y, Li X Y, Zhu Y Y, Liu C M, Wang L, Yu M M, Wei L H, Tang M S & Zhang H Y, *Inorg Chem*, 51 (2012) 12444.
10 Zhou Y, Xiao Y & Qian X H, *Tetrahedron Lett*, 49 (2008) 3380.
11 Ferrand Y, Kendhale A M, Garric J, Kauffmann B & Huc I, *Angew Chem*, 122 (2010) 1822.
12 Hu S Z & Chen C F, *Chem Commun*, 46 (2010) 4199.
13 Gan Q, Ferrand Y, Chandramouli N, Kauffmann B, Aube C, Dubreuil D & Huc I, *J Am Chem Soc*, 134 (2012) 15656.
14 Yamazaki H, Hakamata T, Komi M & Yagi M, *J Am Chem Soc*, 133 (2011) 8846.
15 Tseng H W, Zong R, Muckerman J T & Thummel R, *Inorg Chem*, 47 (2008) 11763.
16 Bhuniya D, Umrani D, Dave B, Salunke D, Kukreja G, Gundu J, Naykodi M, Shaikh N S, Shitole P & Kurhade S, *Bioorg Med Chem Lett*, 21 (2011) 3596.
17 Capozzi A, Mantuano E, Matarrese P, Saccomanni G, Manera C, Mattei V, Gambardella L, Malorni W, Sorice M & Misasi R, *Anti-Cancer Agents Med Chem*, 12 (2012) 653.
18 Chen Y, Li J L, Tong G S M, Lu W, Fu W F, Lai S W & Che C M, *New J Chem*, 2 (2011) 1509.
19 Fernández-Mato A, Quintela J M & Peinador C, *New J Chem*, 36 (2012) 1634.
20 Wu Y Y, Chen Y, Gou G Z, Mu W H, Lv X J, Du M L & Fu W F, *Org Lett*, 14 (2012) 5226.
21 Ligthart G, Ohkawa H, Sijbesma R P & Meijer E, *J Org Chem*, 71 (2006) 375.
22 Anderson C A, Taylor P G, Zeller M A & Zimmerman S C, *J Org Chem*, 75 (2010) 4848.
23 Fu W F, Jia L F, Mu W H, Gan X, Zhang J B, Liu P H, Cao Q Y, Zhang G J, Quan L & Lv X J, *Inorg Chem*, 49 (2010) 4524.
24 Chi S M, Wang Y F, Gan X, Wang D H & Fu W F, *Cent Eur J Chem*, 7 (2009) 923.
25 He C, DuBois J L, Hedman B, Hodgson K O & Lippard S J, *Angew Chem Int Edn*, 40 (2001) 1484.
26 Zhang J F, Fu W F, Gan X & Chen J H, *Dalton Trans*, 23 (2008) 3093.
27 Sheldrich G M, SHELX-97, *Program for the Refinement of Crystal Structures*, (University of Göttingen, Germany) 1997.
28 Connelly N G & Geiger W E, *Chem Rev*, 96 (1996) 877.
29 Ziessel R, Bonardi L, Retailleau P & Ulrich G, *J Org Chem*, 71 (2006) 3093.
30 Poirel A, De Nicola A & Ziessel R, *Org Lett*, 14 (2012) 5696.
31 *Gaussian 09, Rev. B.01*, (Gaussian, Inc., Wallingford CT) 2010.
32 Gou G Z, Zhou B, Shi L, Xu S J, Yan H P, Liu W, and Mang C Y, *Indian J Chem*, 54A (2015) 1017.
33 Patra C N & Ghosh S K, *Indian J Chem*, 39A (2000) 230.
34 Becke A D, *Phys Rev A*, 38 (1988) 3098.
35 Karakaş D & Sayin K, *Indian J Chem*, 52A (2013) 480.
36 Patel R N, Singh Y P, Singh Y & Butcher R J, *Indian J Chem*, 54A (2015) 1459.
37 Hehre W J, Ditchfield R & Pople J A, *J Chem Phys*, 56 (1972) 2257.
38 Francl M M, Pietro W J, Hehre W J, Binkley J S, Gordon M S, DeFrees D J & Pople J A, *J Chem Phys,* 77 (1982) 3654.
39 Krishnan R, Binkley J S, Seeger R & Pople J A, *J Chem Phys*, 72 (1980) 650.
40 Gou G Z, Zhou B, Shi L, Chi S M, Chen X L & Liu W, *Chinese J Chem Phys*, 28 (2015) 695.
41 Dey S, Ghosh K, Halder S, Rizzoli C & Roy P, *Indian J Chem*, 54A (2015) 1451.
42 Miertuš S, Scrocco E & Tomasi J, *Chem Phys*, 55 (1981) 117.
43 Henry R & Hammond P, *J Heterocycl Chem*, 14 (1977) 1109.
44 Chen Y, Fu W F, Li J L, Zhao X J & Ou X M, *New J Chem*, 31 (2007) 1785.
45 Brown E V, *J Org Chem*, 30 (1965) 1607.
46 Paudler W W & Kress T J, *J Org Chem*, 32 (1967) 832.
47 Li Z X, Yu M M, Zhang L F, Yu M, Liu J X, Wei L H & Zhang H Y, *Chem Commun*, 46 (2010) 7169.
48 Wang D P & Ding K, *Chem Commun*, 14 (2009) 1891.
49 Zhang X Y, Dong D Q, Yue T, Hao S H & Wang Z L, *Tetrahedron Lett*, 55 (2014) 5462.
50 Chatterjee S, Bhattacharjee P, Temburu J, Nandi D & Jaisankar P, *Tetrahedron Lett*, 55 (2014) 6680.
51 Xu L, Shao Z, Wang L, Zhao H & Xiao J, *Tetrahedron Lett*, 55 (2014) 6856.
52 Jamal Z, Teo Y C & Wong L K, *Eur J Org Chem*, 2014 (2014) 7343.
53 Jamal Z & Teo Y C, *Synlett*, 25 (2014) 2049.
54 Dujols V, Ford F & Czarnik A W, *J Am Chem Soc*, 119 (1997) 7386.